Rock Mechanics and Rock Engineering
https://doi.org/10.1007/s00603-019-02036-8

ORIGINAL PAPER

# Slip Velocity Dependence of Friction-Permeability Response of Shale Fractures

**Yunzhong Jia[1] · Yi Fang[2] · Derek Elsworth[3] · Wei Wu[1]**

Received: 19 July 2019 / Accepted: 10 December 2019


## Abstract

Fluid injection-induced fracture slip during hydraulic stimulation of shales may be seismic or aseismic with the slip mode potentially influencing the evolution of permeability and subsequent shale gas production. We report a series of friction-permeability tests with constant and stepped velocities on planar saw-cut fractures of Longmaxi shale, Green River shale and Marcellus shale. In particular we explore the additive effect of stepped velocity on fracture permeability evolution relative to the background permeability driven at constant velocity. Fracture permeability decreases at larger slip displacement at constant velocity presumably due to asperity degradation and clay swelling. Sudden up-steps in slip velocity temporarily enhance fracture permeability as a result of shear dilation on hard minerals, but permeability net decreases with increasing slip displacement as wear products fill the pore space. Fracture surface roughness is the link between the fracture permeability and friction coefficient, which are both influenced by mineralogical composition. The fractures and sheared-off particles in the tectosilicate-rich and carbonate-rich shales dilate to increase fracture permeability, whereas asperity comminution readily occurs in the phyllosilicate-rich shale to reduce fracture permeability. The results potentially improve our ability to facilitate shale gas extraction and to mitigate the associated seismic risks.

**Keywords** Shale fracture · Frictional slip · Permeability evolution · Slip velocity

## List of Symbols

| | |
|---|---|
| $\alpha$ | Constant representing effective hydraulic aperture evolution, dimensionless |
| $\Delta P$ | Pore pressure difference between upstream and downstream reservoirs, Pa |
| $\Delta k$ | Change in permeability, $m^2$ |
| $\eta$ | Viscosity of distilled water, Pa·s |
| $\theta^{i+1}$ | State variable after a stepped velocity $V^{i+1}$, dimensionless |
| $\mu^i$ | Friction coefficient at reference velocity $V^i$, dimensionless |
| $A$ | Scanning area, $m^2$ |
| $a$ | Scaling factor representing direct effect in rate-and-state friction laws, dimensionless |
| $b$ | Scaling factor representing evolutionary effect in rate-and-state friction laws, dimensionless |
| $D_c$ | Critical slip distance, m |
| $e_h$ | Effective hydraulic aperture, m |
| $e_{max}$ | Maximum effective hydraulic aperture, m |
| $e_{min}$ | Minimum effective hydraulic aperture, m |
| $k$ | Fracture permeability, $m^2$ |
| $k'$ | Estimated permeability without slip velocity change, $m^2$ |
| $k_{real}$ | Measured permeability after slip velocity change, $m^2$ |
| $k_{trans}$ | Measured permeability before slip velocity change, $m^2$ |
| $L$ | Fracture length, m |
| $Q$ | Flow rate, $m^3/s$ |
| $R_c$ | Contact-area ratio, dimensionless |
| RMS | Root mean square of aperture height, m |
| $S_a$ | Arithmetic mean of aperture height, m |
| $S_z$ | Maximum difference of aperture height, m |
| $W$ | Fracture width, m |
| $z$ | Elevation of scanned point ($x$, $y$) |

✉ Wei Wu
wu.wei@ntu.edu.sg

[1] School of Civil and Environmental Engineering, Nanyang Technological University, Singapore, Singapore

[2] Institute for Geophysics, Jackson School of Geosciences, The University of Texas at Austin, Austin, USA

[3] Department of Energy and Mineral Engineering, EMS Energy Institute, and G3 Center, Pennsylvania State University, University Park, USA

Published online: 20 December 2019

## 1 Introduction

Hydraulic fracturing not only creates new fracture networks to enhance the permeability of shale reservoirs, but also induces frictional slip on pre-existing fractures that may affect the production of shale gas. Elevating the pore pressure during fluid injection can decrease the effective normal stress on shale fractures and result in fracture slip (Guglielmi et al. 2015). Several studies indicate that fracture slip may be seismic or aseismic depending on the asperity population of the fracture surface (Dieterich 1978), the stiffness of the fault and host rock (Leeman et al. 2016; Scholz 1998) and mineralogical composition (Fang et al. 2018b; Ikari et al. 2011; Wang et al. 2017) of the surrounding rock. Seismic slip may result from the shear stress induced by large aseismic deformation (De Barros et al. 2018). The frictional stability of shale fractures is well described by rate-and-state friction laws (Dieterich 1979; Ruina 1983) and associated with the contact state of the fracture surfaces, which can be linked to the evolution of fracture permeability (Ishibashi et al. 2013, 2018; Polak et al. 2003). Shale fractures may dilate or compact during the frictional slip (Fang et al. 2017). Shear-induced permeability enhancement has been reported for rough fractures (Esaki et al. 1999; Fang et al. 2018b), at low effective stress (Wu et al. 2017) and for active dissolution of minerals (Liu et al. 2005; Polak et al. 2004). However, permeability reduction is more commonly observed due to pressure solution (Taron and Elsworth 2010), asperity degradation and the development of gouge materials (Fang et al. 2017) and for the swelling of clays, such as montmorillonite (Jia et al. 2018b).

Rock fractures in tectonic environments typically slip at upper-bound rates of centimeters per year (Ikari and Kopf 2017) and the fracture permeability may thus evolve slowly. Mechanical perturbations (e.g. earthquakes) can unblock pores and cause permeability increases (Elkhoury et al. 2011; Manga et al. 2012; Candela et al. 2014, 2015). Similarly, hydraulic stimulation also perturbs the slip velocity and may result in a change in fracture permeability at stepped velocities (Zoback et al. 2012), which are more complex than that at constant velocity. For example, a sudden change in slip velocity may cause permeability enhancement, leave permeability unchanged, or reduce permeability (Fig. 1), depending on rock type, fracture geometry, stress condition and other factors. During the change in slip velocity, limestone fractures have been shown to exhibit permeability reduction (Zhong et al. 2016) and granite fractures show permeability enhancement (Im et al. 2017; Ishibashi et al. 2018). The permeability variation is strongly influenced by asperity damage and gouge generation. Fracture permeability in shale decreases exponentially to a static state over a certain displacement regardless of constant-velocity or stepped-velocity conditions (Fang et al. 2017). These studies indicate that the permeability evolution due to velocity change depends on both slip mode and mineralogical composition. However, the influence of injection-induced stepped velocity on fracture permeability remains unclear, which may be different from the fracture permeability controlled by constant velocity associated with tectonic deformation. Understanding the influence of stepped velocity on fracture permeability in shale is critical to improve shale gas production and to mitigate the risk of induced geohazards.

We report a series of observations of friction-permeability evolution driven at both constant- and stepped-velocities to characterize the permeability evolution of shale fractures. We concurrently record the evolution of friction coefficient and fracture permeability and carefully examine the differences resulting from driving response under constant- and stepped-velocities. Finally, we discuss the relation between permeability response and friction rate parameters based on asperity degradation and contact-area

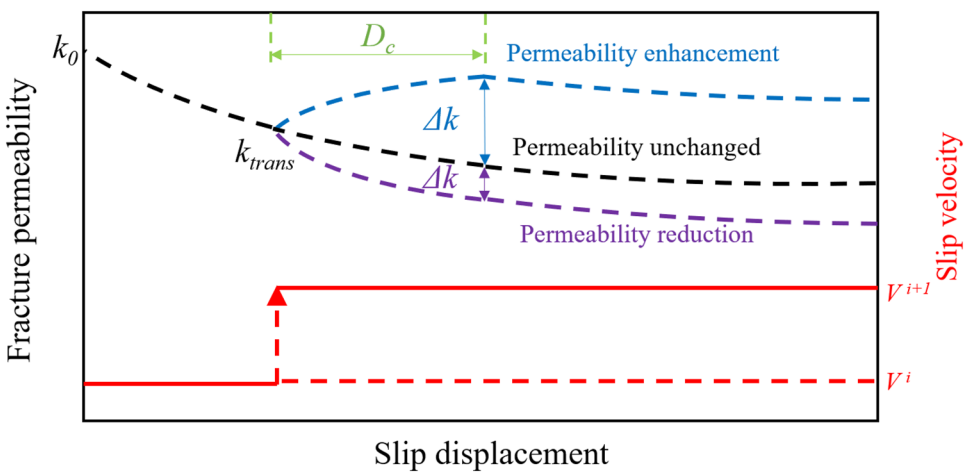


**Fig. 1** Schematic diagram showing possible permeability response to a change in slip velocity (modified from Ishibashi et al. 2018)

ratio and in particular address the link between the fracture permeability and friction strength.

## 2 Experimental Method

We performed concurrent measurements of the evolution of friction and permeability with shear offset on fractures of shale with three different mineral compositions. We constrained these measurements with pre- and post-test measurements of fracture roughness to define key processes.

### 2.1 Sample Preparation

We drilled 12 cylindrical core samples perpendicular to the bedding planes from three types of intact shales—Longmaxi shale, Green River shale and Marcellus shale. The Longmaxi shale is a siliceous dolomitic shale (Jiang et al. 2013) and was collected from an outcrop of the Silurian Longmaxi Formation in Sichuan, China. The freshwater lacustrine Green River shale was obtained from Grand Junction, Colorado. The Marcellus shale was extracted from an outcrop of Middle Devonian Marcellus formation in Pennsylvania. The mineralogical compositions of the three shales were determined by powder X-ray diffraction analysis (Table 1). These

**Table 1** Mineralogical compositions of Longmaxi shale, Green River shale and Marcellus shale (Jia et al. 2018b) and Mohs hardness of rock-forming minerals (Whitney et al. 2007)

| Mineral group | Mineral | Longmaxi shale | Green River shale | Marcellus shale | Mohs hardness |
|---|---|---|---|---|---|
| Tectosilicate | Quartz | 51.6% | 14.9% | 36.1% | 7.0–7.5 |
| | Feldspar | 0 | 24.5% | 0 | 5.0–6.5 |
| | Albite | 3.7% | 0 | 0 | 6.0–6.5 |
| | Microcline | 0 | 6.5% | 0 | 6.0–6.5 |
| Carbonate | Dolomite | 3.4% | 39.4% | 0 | 3.5–4.0 |
| | Calcite | 16.7% | 12.4% | 0 | 3.0–3.5 |
| Phyllosilicate | Muscovite | 0 | 0 | 10.4% | 2.0–2.5 |
| | Illite | 24.6% | 2.3% | 37.4% | 1.0–2.0 |
| | Chlorite | 0 | 0 | 0 | 2.0–2.5 |
| | Kaolinite | 0 | 0 | 4.9% | 2.0–2.5 |
| | Montmorillonite | 0 | 0 | 11.2% | 1.5–2.0 |

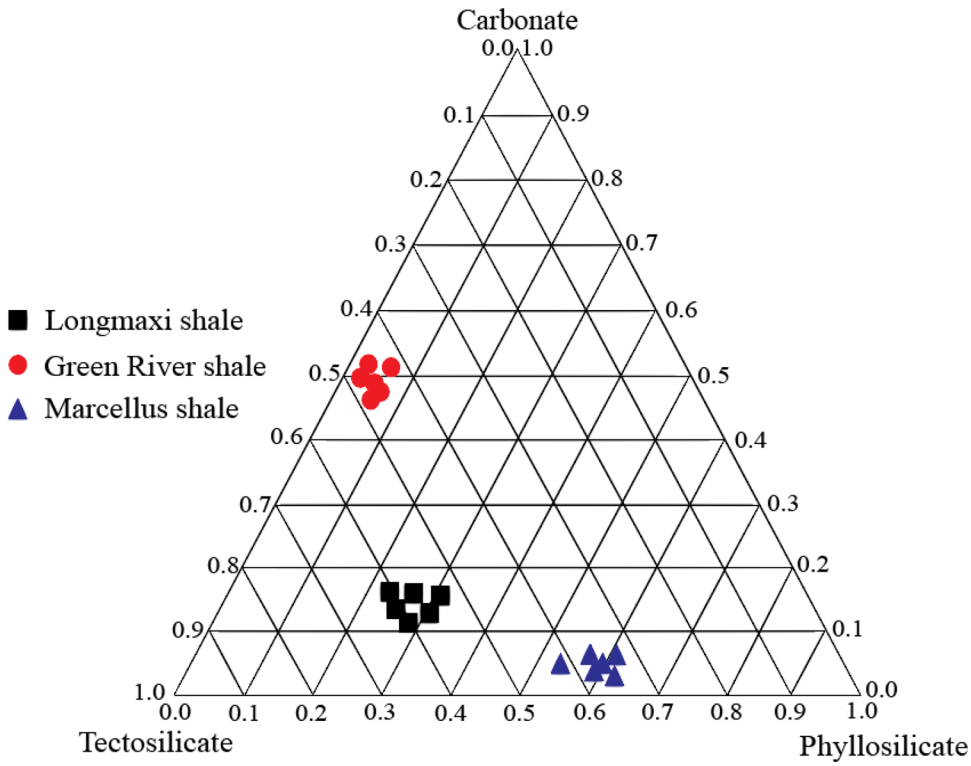


**Fig. 2** Mineralogical composition of Longmaxi shale, Green River shale and Marcellus shale

shales are comprised of three principal mineral groups: tectosilicates (e.g. quartz, feldspar and albite), carbonates (e.g. calcite and dolomite) and phyllosilicates (e.g. illite, chlorite and kaolinite). Figure 2 shows the classification of the shale lithofacies in a ternary diagram. The Mohs hardness of the minerals are summarized in Table 1 (Whitney et al. 2007), and the average Mohs hardness of Longmaxi shale, Green River shale and Marcellus shale are 5.5, 5.0 and 2.5, respectively. Table 2 lists the physical and mechanical properties of Longmaxi shale, Green River shale and Marcellus shale, respectively. We bisected the core sample (25.2 mm in diameter and 50.4 mm in length) into two halves along the core axis using a diamond saw and polished the fracture surfaces using #20 grit silicon carbide. Thus, the slip direction is perpendicular to the bedding planes.

## 2.2 Experimental Setup

We used a triaxial cell to conduct the friction-permeability tests (Fig. 3). The core sample with a fracture was stabilized by a rubber sleeve and sealed by Teflon tape at the sleeve ends to prevent fluid leakage. An aluminum sleeve was then used to cover the load cell to eliminate the effect of confining pressure on axial stress measurement. The initial offset of the sample halves was 6 mm with this offset length reserved for shear movement. The gaps between the sample halves and forcing blocks were filled with soft and inert plastic filler. The slip displacement was measured using a linear variable displacement transducer (LVDT) with an accuracy of ±0.01 μm. Three ISCO 500D pumps were used in the tests. Pump A and Pump B controlled the confining pressure (i.e. the normal stress on the fracture) and axial stress (i.e. the shear stress on the fracture), respectively, using hydrogenated oil. The pore pressure was applied through Pump C using distilled water. More details regarding the experimental setup can be found in Fang et al. (2017, 2018a). In the permeability measurement, we held a constant pressure difference, $\Delta P$ [Pa], between the upstream and downstream reservoirs and monitored the flow rate of Pump C, $Q$ [$m^3/s$]. The downstream reservoir was connected to the atmosphere. The fracture permeability, $k$ [$m^2$], was calculated according to the cubic law as (Witherspoon et al. 1980; Zimmerman and Yeo 2000):

**Table 2** Physical and mechanical properties of Longmaxi shale, Green River shale and Marcellus shale

| Property | Longmaxi shale | Green river shale | Marcellus shale |
|---|---|---|---|
| Uniaxial compressive strength (MPa) | 136.0 | 83.5 | 58.6 |
| Tensile strength (MPa) | 13.5 | 9.3 | 6.6 |
| Young's modulus (GPa) | 25.0 | 14.4 | 12.6 |
| Bulk modulus (GPa) | 16.7 | 10.3 | 8.6 |
| Possion's ratio | 0.25 | 0.20 | 0.23 |
| Porosity | 3.9% | 8.2% | 9.5% |
| Matrix permeability ($m^2$) | $10^{-20}$ | $10^{-18}$ | $10^{-18}$ |

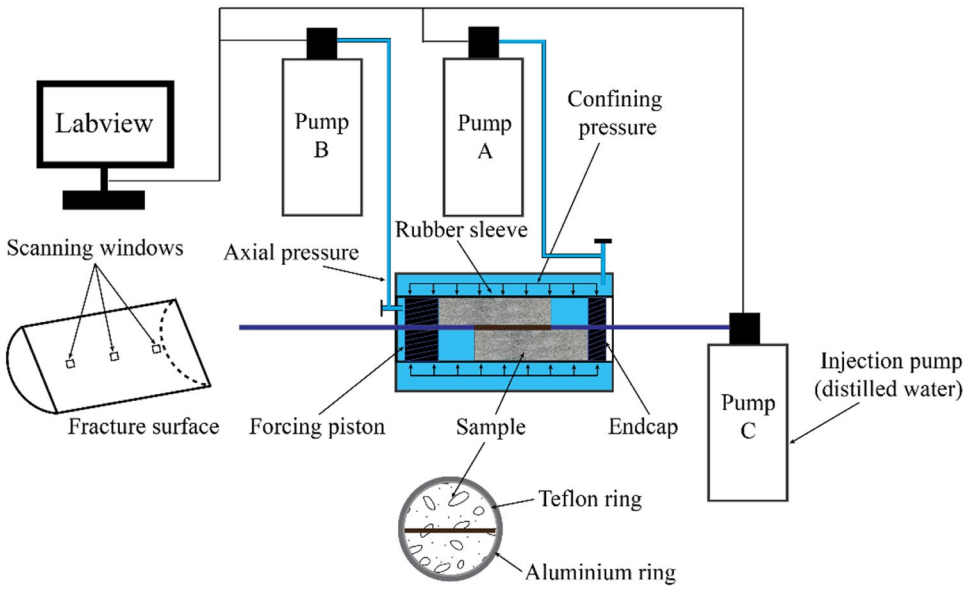


**Fig. 3** Friction-permeability experimental setup

$$e_{\mathrm{h}} = \left(-\frac{12\eta LQ}{W\Delta P}\right)^{\frac{1}{3}} \tag{1}$$

$$k = \frac{e_{\mathrm{h}}^2}{12} \tag{2}$$

where $e_h$ [m] is the effective hydraulic aperture; $\eta$ [Pa s] is the viscosity of distilled water; and $L$ [m] and $W$ [m] are the length and width of the fracture, respectively.

A Zygo NewView optical profilometer was used to scan the fracture surfaces both before and after the tests and to evaluate the change in topography of fracture surfaces. The vertical and horizontal resolutions are 1.0 nm and 1.6 µm, respectively. We chose three windows with a dimension of 1.68 mm × 1.68 mm along the shear direction (Fig. 3). Based on the scanned data, we obtained the arithmetic mean ($S_a$), root mean square (RMS) and maximum difference ($S_z$) of asperity height to characterize fracture surface roughness (Brown 1987; Candela et al. 2009):

$$S_{\mathrm{a}} = \frac{1}{A}\int |z(x,y)|\mathrm{d}x\mathrm{d}y \tag{3}$$

$$\mathrm{RMS} = \frac{1}{A^2}\iint z^2(x,y)\mathrm{d}x\mathrm{d}y \tag{4}$$

where $z$ [m] is the elevation of scanned point ($x$, $y$); $A$ [m$^2$] is the scanning area. The values of $S_a$, RMS and $S_z$ given in Table 3 are the average calculated based on the data collected from three scanning windows.

## 2.3 Experimental Procedure

The friction-permeability tests were performed on the shale fractures at room temperature (25 °C). In the constant-velocity friction tests, we first applied 3 MPa confining pressure and 120 kPa pore pressure until the fracture was fully saturated with distilled water. The fracture was then sheared at a constant velocity of 10 µm/s until the slip displacement reached 5 mm (Fig. 4). The normal and shear stresses were recorded to calculate the friction coefficient, and the fracture permeability was also measured during the displacement process. In the stepped-velocity friction tests at 3 MPa confining pressure and 120 kPa pore pressure, the fully saturated fracture was first sheared at a constant velocity of 10 µm/s until the friction coefficient was stable. Three slip velocities (i.e. 1, 5 and 10 µm/s) were subsequently switched between both down-steps (from high velocity to low velocity) and up-steps (from low velocity to high velocity) until the slip

**Table 3** Arithmetic mean ($S_a$), root mean square (RMS) and maximum difference ($S_z$) of asperity height before and after constant-velocity friction experiments

| Shale fracture | $S_a$ before/after test (µm) | RMS roughness before/after test (µm) | $S_z$ before/after test (µm) |
|---|---|---|---|
| Longmaxi-1 | 6.42/4.09 | 8.34/5.52 | 53.54/48.55 |
| Longmaxi-2 | 6.78/4.25 | 8.95/5.24 | 55.22/46.33 |
| Green River-1 | 7.90/4.95 | 9.68/6.02 | 66.72/48.54 |
| Green River-2 | 7.62/4.71 | 9.33/5.94 | 68.52/49.80 |
| Marcellus-1 | 8.83/3.15 | 11.17/4.33 | 62.93/26.51 |
| Marcellus-2 | 8.99/3.27 | 11.44/4.68 | 65.55/28.17 |

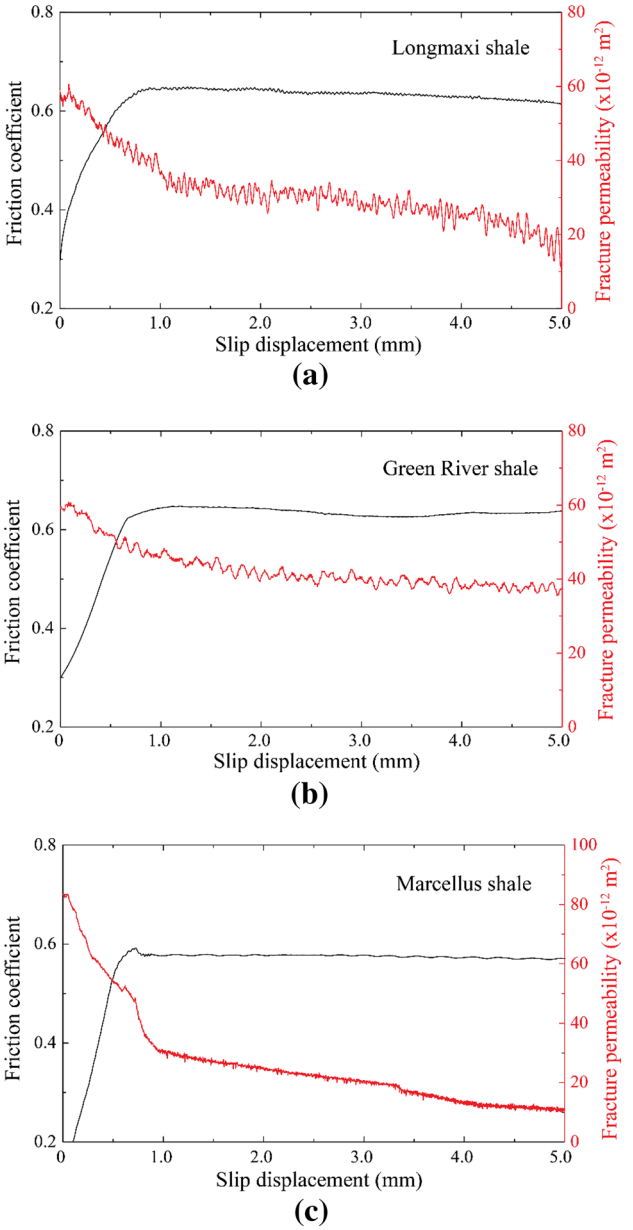


**Fig. 4** Friction coefficient and fracture permeability as a function of slip displacement in constant-velocity friction experiments on **a** Longmaxi shale, **b** Green River shale and **c** Marcellus shale

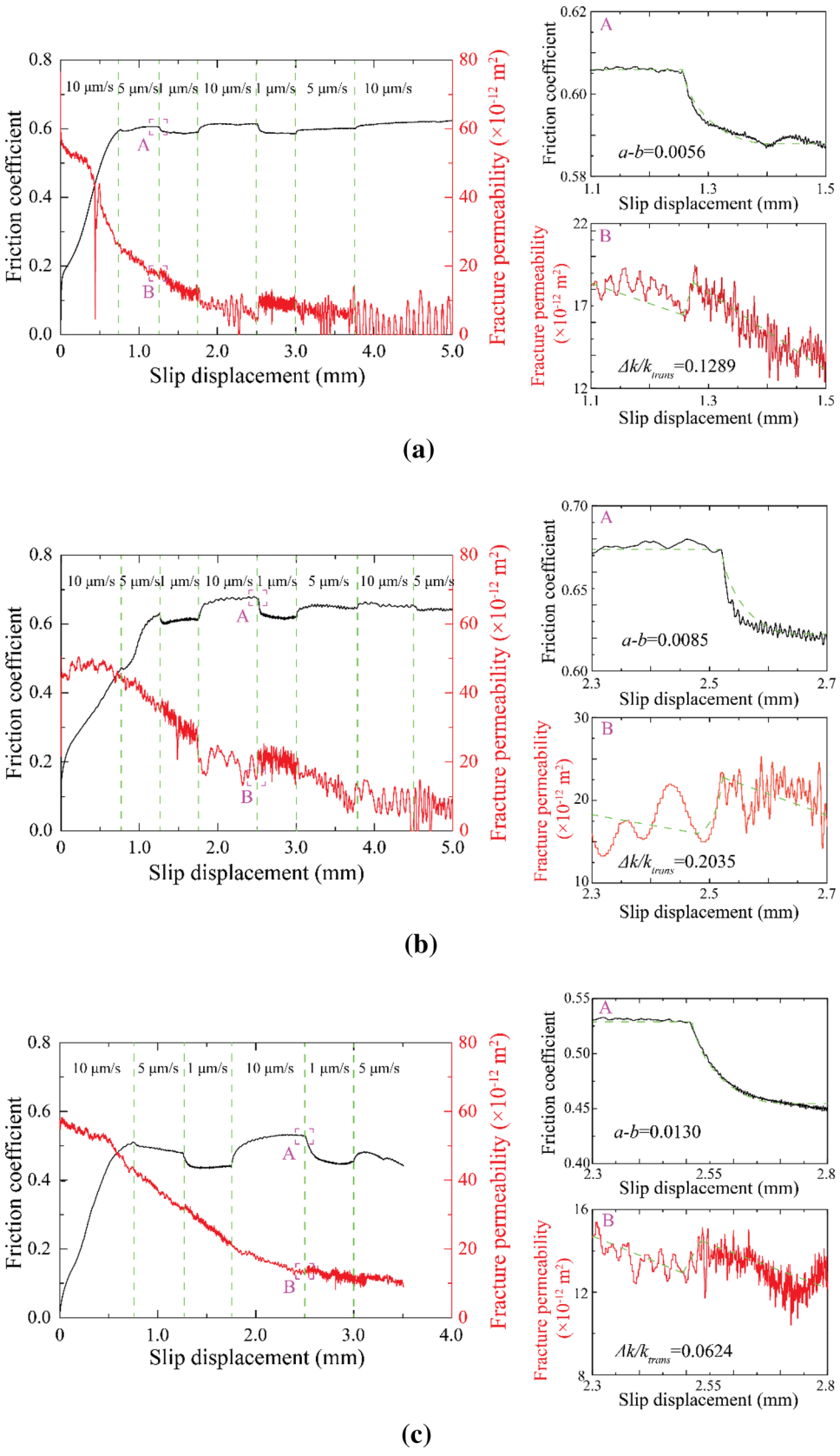


**Fig. 5** Friction coefficient and fracture permeability as a function of slip displacement in stepped-velocity friction experiments on **a** Longmaxi shale, **b** Green River shale and **c** Marcellus shale

displacement reached ~ 5 mm (Fig. 5). We also repeated the stepped-velocity friction tests to verify repeatability of the measured changes in friction and fracture permeability.

## 3 Experimental Results

We first report experimental observations of friction-permeability evolution during constant-velocity slip. Then, we summarize how the rate-dependent friction parameter and permeability response evolve during stepped-velocity slip.

### 3.1 Permeability Evolution During Constant-Velocity Friction Tests

The friction coefficient is obtained from the ratio of the shear stress to normal stress. The fracture permeability is calculated from Eqs. (1) and (2). Figure 4 shows the friction coefficient and fracture permeability as a function of slip displacement during the constant-velocity friction tests on the shale fractures. At a constant velocity of 10 μm/s, the friction coefficient increases linearly with larger slip displacement and subsequently remains relatively stable after the friction coefficient reaches the peak value. The friction coefficients of the Longmaxi shale and Green River shale evolve in a similar manner, but are larger than that of the Marcellus shale fracture at the same slip displacement. Our results are in accordance with other studies that the friction coefficient increases with higher tectosilicate content (Ikari et al. 2011; Kohli and Zoback 2013; Fang et al. 2017; Zhang et al. 2019), as less clay-rich and platy-grain gouge materials are produced from the slip process.

Before fracture slip, the initial permeability of fractures in the Longmaxi shale, Green River shale and Marcellus shale are $58.80\times10^{-12}$ m$^2$, $59.11\times10^{-12}$ m$^2$ and $83.55\times10^{-12}$ m$^2$, respectively. The profilometer results show that the RMS value of the Marcellus shale fracture is larger than that of the Longmaxi and Green River shale fractures (Table 3). The rougher fracture surface is scratched more deeply by the hard silicon carbide may provide more fluid flow pathways and thus result in higher fracture permeability (Li et al. 2008; Jia et al. 2018a). The permeability of the three shale fractures increases slightly within the first 0.1 mm slip displacement due to asperity dilation and deformation before the damage occurs (Fang et al. 2018a, b). The permeability subsequently decreases with further slip displacement. The fracture permeability continuously decreases before the friction coefficient peaks and retains this downward trend after the peak value. The permeability of the Longmaxi shale fracture finally decreases to $19.82\times10^{-12}$ m$^2$, the permeability of the Green River shale fracture reduces to $37.68\times10^{-12}$ m$^2$, and the permeability of the Marcellus shale fracture exhibits the largest permeability drop to $10.31\times10^{-12}$ m$^2$.

### 3.2 Permeability Evolution During Stepped-Velocity Friction Tests

We use the rate-and-state friction laws to describe the friction coefficient in the stepped-velocity friction tests. The friction coefficient, $\mu$ [dimensionless], is expressed as (Marone 1997):

$$\mu(V,\theta)=\mu^{i}+a\ln\left(\frac{V^{i+1}}{V^{i}}\right)+bln\left(\frac{V^{i}\theta^{i+1}}{D_{\mathrm{c}}^{i+1}}\right) \tag{5}$$

$$\frac{d\theta^{i+1}}{dt}=1-\frac{V^{i+1}\theta^{i+1}}{D_{c}^{i+1}} \tag{6}$$

where $\mu^{i}$ is the friction coefficient at a reference velocity $V^{i}$ [μm/s]; $\theta^{i+1}$ [dimensionless] is the state variable after the velocity is stepped to $V^{i+1}$ [μm/s]; $a$ and $b$ are the frictional parameters, which represent the direct and evolutionary effects of velocity change, respectively; and $D_{\mathrm{c}}^{i+1}$ [μm] is the critical slip distance, over which a new steady state is established at the stepped velocity.

Slip instability is indexed by the frictional rate parameter ($a$–$b$) derived from Eq. (5):

$$(a-b)=\frac{(\mu^{i+1}-\mu^{i})}{\ln(V^{i+1}/V^{i})}. \tag{7}$$

A positive value of ($a$–$b$) indicates that the fracture is velocity-strengthening and intrinsically stable. In contrast, when ($a$–$b$) is negative, the fracture exhibits velocity-weakening behavior and is unstable or conditionally stable, depending on whether the effective normal stress reaches a critical value.

We also use the permeability response parameter ($\Delta k/k_{\mathrm{trans}}$) to quantitatively assess the instantaneous change in fracture permeability (Fang et al. 2018b; Ishibashi et al. 2018):

$$\Delta k/k_{\mathrm{trans}}=\frac{k_{\mathrm{real}}-k'}{k_{\mathrm{trans}}} \tag{8}$$

where $k_{\mathrm{trans}}$ [m$^2$] and $k_{\mathrm{real}}$ [m$^2$] are the measured permeabilities before and after the stepped-velocity friction tests, respectively; and $k'$ [m$^2$] is the estimated permeability without velocity change obtained from the constant-velocity friction tests.

As shown in Fig. 5, the friction coefficient initially increases as the slip displacement increases. When the friction coefficient is relatively stable, the friction coefficient increases with an up-step in the slip velocity and decreases with a down-step. The fracture permeability generally decreases with larger slip displacement, which is similar to the results obtained from the

constant-velocity friction tests. However, the fracture permeability increases slightly due to the sudden up-step in slip velocity (Fig. 5 inset). Table 4 summaries the friction rate parameter and permeability response in the velocity-stepped friction tests. The shale fractures exhibit velocity-strengthening behaviors regardless of mineralogical composition. The permeability of the shale fractures is enhanced, except for three cases of the Marcellus shale fracture. Figure 6 demonstrates the relationship between the mineralogical composition and permeability evolution of the shale fractures. The results reveal that the permeability of the Marcellus shale fracture is less dependent on mineralogical composition as it shows a minimal variation in permeability in response to this parameter.

## 4 Discussion

The constant-velocity friction test results show that the mineralogical composition significantly influences the friction and permeability evolution of shale fractures. This influence can be clearly observed during the early stage of fracture slip. The friction coefficient increases with larger slip displacement, which is accompanied by asperity degradation. The changes in $S_a$, RMS and $S_z$ indicate that the Marcellus shale fractures experience more severe wear than the other fractures (Table 3). The fracture asperities in the phyllosilicate-rich shale containing a significant proportion of soft minerals readily comminute, leading to a sharp reduction in fracture permeability. Particularly, the relatively high content of clay minerals (e.g. muscovite, illite, kaolinite and montmorillonite) in the Marcellus shale promotes the reduction in fracture permeability. The clay minerals absorb

**Table 4** Friction rate parameter and permeability response parameter obtained from velocity-stepped friction experiments

| Shale fracture | Step sequence | Shear velocity (μm/s) | Friction rate parameter ($a$–$b$) | Permeability response parameter ($\Delta k/k_{trans}$) |
|---|---|---|---|---|
| Longmaxi-3 | 1 | 10.0–5.0 | 0.0113 | 0.0915 |
| | 2 | 5.0–1.0 | 0.0026 | 0.2961 |
| | 3 | 1.0–10.0 | 0.0081 | 0.1142 |
| | 4 | 10.0–1.0 | 0.0082 | 0.1640 |
| | 5 | 1.0–5.0 | 0.0175 | 0.0894 |
| Longmaxi-4 | 1 | 10.0–5.0 | 0.0019 | 0.2841 |
| | 2 | 5.0–1.0 | 0.0056 | 0.1289 |
| | 3 | 1.0–10.0 | 0.0047 | 0.0502 |
| | 4 | 10.0–1.0 | 0.0188 | 0.0294 |
| | 5 | 1.0–5.0 | 0.0006 | 0.2351 |
| Green river-3 | 1 | 10.0–5.0 | 0.0052 | 0.2864 |
| | 2 | 5.0–1.0 | 0.0050 | 0.2215 |
| | 3 | 1.0–10.0 | 0.0110 | 0.0549 |
| | 4 | 10.0–1.0 | 0.0145 | 0.0075 |
| | 5 | 1.0–5.0 | 0.0111 | 0.0265 |
| Green river-4 | 1 | 10.0–5.0 | 0.0086 | 0.2235 |
| | 2 | 5.0–1.0 | 0.0051 | 0.2653 |
| | 3 | 1.0–10.0 | 0.0126 | 0.0078 |
| | 4 | 10.0–1.0 | 0.0085 | 0.2035 |
| | 5 | 1.0–5.0 | 0.0064 | 0.2479 |
| Marcellus-3 | 1 | 10.0–5.0 | 0.0171 | −0.0457 |
| | 2 | 5.0–1.0 | 0.0178 | −0.1246 |
| | 3 | 1.0–10.0 | 0.0144 | 0.0486 |
| | 4 | 10.0–1.0 | 0.0130 | 0.0624 |
| | 5 | 1.0–5.0 | 0.0092 | 0.2204 |
| Marcellus-4 | 1 | 10.0–5.0 | 0.0085 | 0.1894 |
| | 2 | 5.0–1.0 | 0.0075 | 0.2017 |
| | 3 | 1.0–10.0 | 0.0102 | −0.1543 |
| | 4 | 10.0–1.0 | 0.0124 | 0.0413 |
| | 5 | 1.0–5.0 | 0.0108 | 0.1526 |

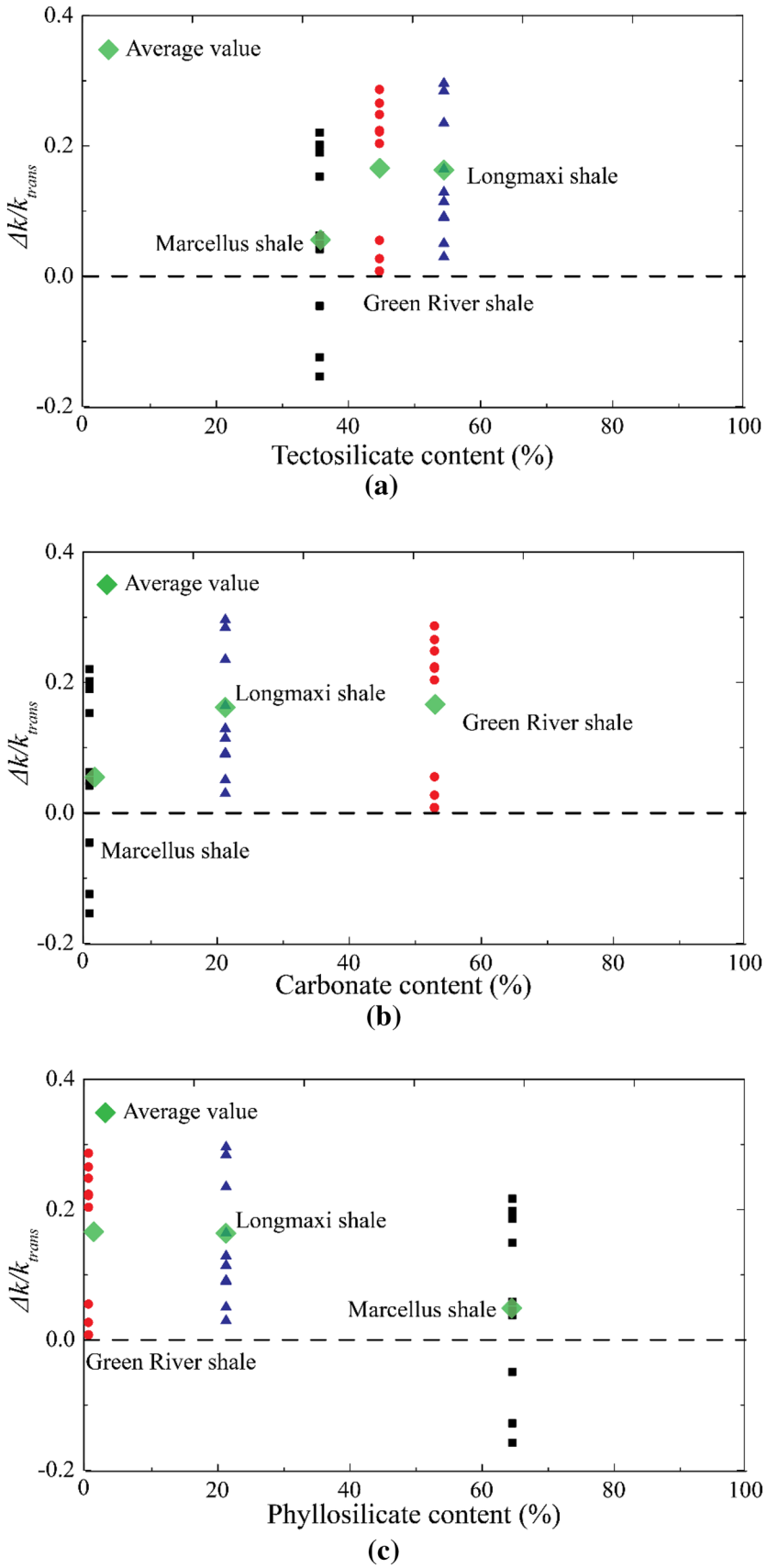


**Fig. 6** Permeability evolution parameter ($\Delta k/k_{trans}$) as a function of **a** tectosilicate content, **b** carbonate content and **c** phyllosilicate content

water and expand to reduce the hydraulic aperture (Chenevert 1970; Jia et al. 2018b). However, the fracture asperities in the tectosilicate-rich and carbonate-rich shales are mainly composed of hard minerals that resist degradation, showing only a minor change in fracture permeability. The minor change may also result from the opposite impact of fracture dilation, by which the fracture surfaces override (Im et al. 2018) and thus restricts the permeability reduction. In the velocity-stepped friction tests, the reductions in fracture permeability fluctuate significantly and without an obvious pattern, presumably due to the complex frictional behaviors of the produced gouges during the sudden velocity change and potentially influenced by the slow response of the ISCO pumps.

Figure 7 shows that the RMS magnitude, permeability and friction coefficient of the three shales all decrease following the constant-velocity friction tests. The fracture in the phyllosilicate-rich shale exhibits larger reductions in RMS and permeability than those in the tectosilicate-rich and carbonate-rich shales. For each fracture, the friction coefficient decreases with increasing RMS, congruent with other studies (Marone and Cox 1994; Fang et al. 2018a). However, the fracture with a larger RMS value in the phyllosilicate-rich shale does not exhibit a greater decline in friction coefficient. This is probably because the mineralogical composition plays a more important role in the slip behaviors of the three polished fractures. The fracture surface roughness is likely a key link between fracture permeability and friction coefficient.

As slip displacement further increases, the friction coefficient remains stable in the constant-velocity friction tests as the fracture permeability constantly decreases. Sheared-off particles in the fractures further promote permeability reduction. Soft particles are readily plucked from the fracture surfaces and subsequently crushed in the frictional process. Although the fracture may dilate due to the uplift and rotation of hard particles, crushed particles will occlude the pore space and eventually result in permeability reduction (Fang et al. 2016). This explanation is congruent with the reduction in fracture permeability observed in the phyllosilicate-rich shale with a high clay mineral content.

In the velocity-stepped friction tests, the fracture permeability slightly increases with a sudden change in slip velocity, but constantly decreases with a further increase in slip displacement at the same slip velocity. The increase in slip velocity likely causes shear dilation by the overriding of hard particles and temporarily enhances fracture permeability. However, the cumulative effect of velocity-stepped on fracture permeability is minor compared to the dominant impact of permeability controlled by the constant velocity. Figure 8a shows that the permeability response parameter is independent of the velocity stepped ratio, ln ($V^{i+1}/V^{i}$). Our data also show that the permeability decreases with a larger friction rate parameter (Fig. 8b). Similar trends are observed in other studies (Fang et al. 2018a; Ishibashi et al. 2018). Permeability evolution can be interpreted through the contact characteristics of fracture surfaces. Based on the cubic law (Zimmerman et al. 1992), the fracture permeability is associated with effective hydraulic aperture, $e_h$ [m], which can be expressed as (Yasuhara 2004):

$$e_h = (e_{max} - e_{min}) \times \exp(-R_c/\alpha) \tag{9}$$

where $e_{max}$ [m] and $e_{min}$ [m] are the maximum and minimum effective hydraulic apertures, respectively; $R_c$ [dimensionless] is the ratio of the contact area to fracture area, also known as the contact-area ratio; and the constant $\alpha$ [dimensionless] can be determined by core flooding experiments.

Permeability reduction is also associated with the increase in contact-area ratio (Gangi and Carlson 1996; Yasuhara et al. 2006). The mineral hardness could be a bridge linking among the frictional strength, rate-dependent parameter and permeability response parameter. Among the three fractures, the fractures in the phyllosilicate-rich shale containing lower

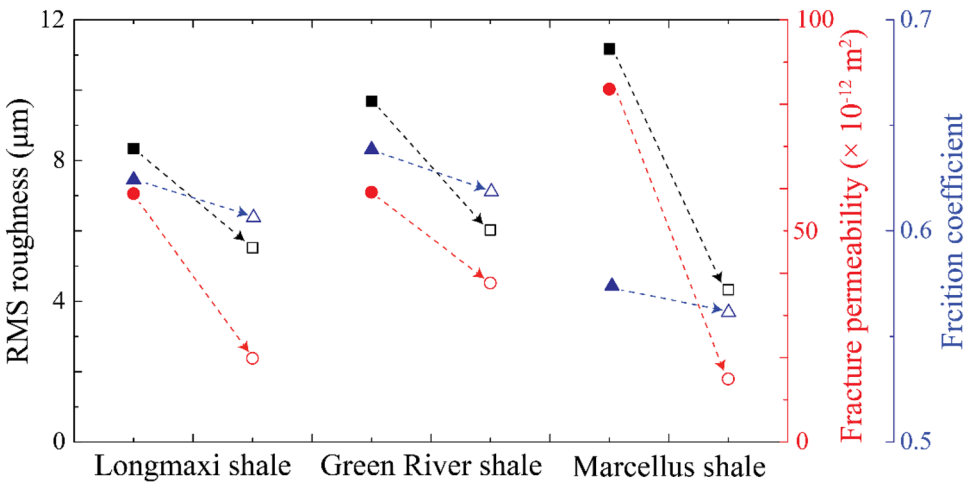


**Fig. 7** RMS roughness, fracture permeability and friction coefficient before (solid symbols) and after (open symbols) constant-velocity friction experiments on Longmaxi shale, Green River shale and Marcellus shale

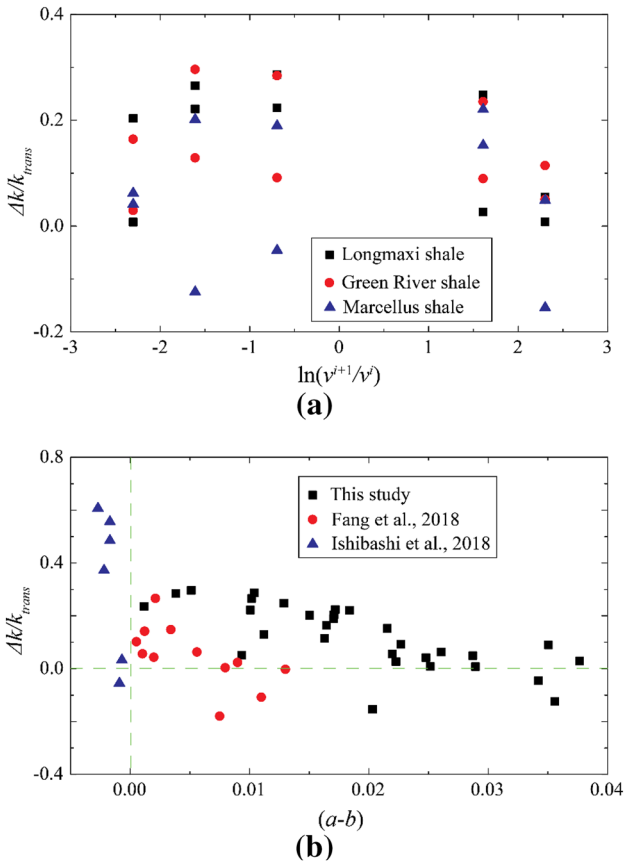


**Fig. 8** Permeability response parameter ($\Delta k/k_{trans}$) as a function of **a** velocity stepped ratio [ln ($V^{i+1}/V^i$)] and **b** friction rate parameter ($a$–$b$)

hardness minerals always show lower frictional strength and larger rate-dependent parameter. This observation is consistent with previous research (Moore and Lockner 2011; Samuelson and Spiers 2012; Kohli and Zoback 2013; Verberne et al. 2014). A sudden change in slip velocity perturbs the initial steady state of the fracture. The fracture accommodates this perturbation and stabilizes in a new steady state. The soft minerals in the phyllosilicate-rich shale collapse with an increase in the contact-area ratio, which decreases the effective hydraulic aperture and promotes fracture permeability reduction. In contrast, the hard minerals in the tectosilicate-rich and carbonate-rich shales promote shear dilation with a decrease in the contact-area ratio, enlarging the effective hydraulic aperture and enhancing fracture permeability. Therefore, controlling contact-area ratio has the potential to improve shale gas production. In phyllosilicate-rich shale reservoirs, adding proppants in hydraulic fracturing fluids can potentially restrain the increase in contact-area ratio. Fracture slip in tectosilicate-rich and carbonate-rich shale reservoirs can promote permeability, but the contact-area ratio needs to be well managed to avoid uncontrollable seismic events (Elsworth et al. 2016).

## 5 Conclusion

We investigate the permeability evolution of shale fractures under constant-velocity and velocity-stepped conditions. Our results indicate systematic permeability reduction with increasing slip displacement at constant velocity. However, sudden changes in slip velocity can slightly enhance fracture permeability. The permeability evolution can be interpreted as controlled by the evolving contact-area ratio, which increases with asperity degradation and larger effective hydraulic aperture and decreases with shear dilation and smaller aperture size. All shale fractures examined in this study show velocity-strengthening behavior. The velocity-stepped friction test results also show that the fractures in the tectosilicate-rich and carbonate-rich shales exhibit permeability enhancement, while the fracture permeability in the phyllosilicate-rich shale changes independent of velocity change due to relatively high clay content and low carbonate content. This study improves our understanding of the link between fracture slip and permeability evolution under varying shear velocity conditions, which suggests that effectively controlling the ratio of the contact area to fracture area can help improve shale gas production. Our data also reveal that special considerations associated with shale mineralogy and fracture contact-area ratio (e.g., adding proppants or chemical additives) are needed in hydraulic fracturing to improve shale gas production (especially in clay-rich shale reservoirs) and to mitigate anthropogenic seismic events (especially on critically stressed fractures).

## Compliance with Ethical Standards

**Conflict of interest** The authors declare no conflict of interest.

## References

Brown SR (1987) Fluid flow through rock joints: the effect of surface roughness. J Geophys Res 92(B2):1337–1347

Candela T, Renard F, Bouchon M, Brouste A, Marsan D, Schmittbuhl J, Voisin C (2009) Characterization of fault roughness at various scales: implications of three-dimensional high resolution topography measurements. Pure Appl Geophys 166(10–11):1817–1851

Candela T, Brodsky EE, Marone C, Elsworth D (2014) Laboratory evidence for particle mobilization as a mechanism for permeability enhancement via dynamic stressing. Earth Planet Sci Lett 392:279–291

Candela T, Brodsky EE, Marone C, Elsworth D (2015) Flow rate dictates permeability enhancement during fluid pressure oscillations in laboratory experiments. J Geophys Res Solid Earth 120(4):2037–2055

Chenevert ME (1970) Shale alteration by water adsorption. J Pet Technol 22(09):1141–1148

De Barros L, Guglielmi Y, Rivet D, Cappa F, Duboeuf L (2018) Seismicity and fault aseismic deformation caused by fluid injection in decametric in situ experiments. Com Rend Geosci 350:464–475

Dieterich JH (1978) Time-dependent friction and the mechanics of stick-slip. Pure Appl Geophys 116(4–5):790–806

Dieterich JH (1979) Modeling of rock friction: 1. Experimental results and constitutive equations. J Geophys Res Solid Earth 84(5):2161–2168

Elkhoury JE, Niemeijer A, Brodsky EE, Marone C (2011) Laboratory observations of permeability enhancement by fluid pressure oscillation of in situ fractured rock. J Geophys Res Solid Earth 116:B02311

Elsworth D, Spiers CJ, Niemeijer AR (2016) Understanding induced seismicity. Science 354(6318):1380–1381

Esaki T, Du S, Mitani Y, Kusada K, Jing L (1999) Development of a shear-flow test apparatus and determination of coupled properties for a single rock joint. Int J Rock Mech Min Sci 36(5):641–650

Fang Y, den Hartog SA, Elsworth D, Marone C, Cladouhos T (2016) Anomalous distribution of microearthquakes in the Newberry Geothermal Reservoir: mechanisms and implications. Geothermics 63:62–73

Fang Y, Elsworth D, Wang C, Ishibashi T, Fitts JP (2017) Frictional stability-permeability relationships for fractures in shales. J Geophys Res Solid Earth 122(3):1760–1776

Fang Y, Elsworth D, Ishibashi T, Zhang F (2018a) Permeability evolution and frictional stability of fabricated fractures with specified roughness. J Geophys Res Solid Earth 123(11):9355–9375

Fang Y, Elsworth D, Wang C, Jia Y (2018b) Mineralogical controls on frictional strength, stability, and shear permeability evolution of fractures. J Geophys Res Solid Earth 123(5):3549–3563

Gangi AF, Carlson RL (1996) An asperity-deformation model for effective pressure. Tectonophysics 256:241–251

Guglielmi Y, Cappa F, Avouac JP, Henry P, Elsworth D (2015) Seismicity triggered by fluid injection-induced aseismic slip. Science 348(6240):1224–1226

Ikari MJ, Kopf AJ (2017) Seismic potential of weak, near-surface faults revealed at plate tectonic slip rates. Sci Adv 3:e1701269

Ikari MJ, Marone C, Saffer DM (2011) On the relation between fault strength and frictional stability. Geology 39(1):83–86

Im K, Elsworth D, Marone C, Leeman J (2017) The impact of frictional healing on stick-slip recurrence interval and stress drop: implications for earthquake scaling. J Geophys Res Solid Earth 122(12):10102–10117

Im K, Elsworth D, Fang Y (2018) The influence of preslip sealing on the permeability evolution of fractures and faults. Geophys Res Lett 45(1):166–175

Ishibashi T, McGuire TP, Watanabe N, Tsuchiya N, Elsworth D (2013) Permeability evolution in carbonate fractures: competing roles of confining stress and fluid pH. Water Resour Res 49(5):2828–2842

Ishibashi T, Elsworth D, Fang Y, Riviere J, Madara B, Asanuma H, Watanabe N, Marone C (2018) Friction-stability-permeability evolution of a fracture in granite. Water Resour Res 54(12):9901–9918

Jia Y, Lu Y, Elsworth D, Fang Y, Tang J (2018a) Surface characteristics and permeability enhancement of shale fractures due to water and supercritical carbon dioxide fracturing. J Pet Sci Eng 165:284–297

Jia Y, Lu Y, Tang J, Fang Y, Xia B, Ge Z (2018b) Mechanical-chemical-mineralogical controls on permeability evolution of shale fractures. Geofluids 2018:7801843

Jiang Z, Guo L, Liang C (2013) Lithofacies and sedimentary characteristics of the Silurian Longmaxi Shale in the southeastern Sichuan Basin. China. J Palaeogeogr 2(3):238–251

Kohli AH, Zoback MD (2013) Frictional properties of shale reservoir rocks. J Geophys Res Solid Earth 118(9):5109–5125

Leeman JR, Saffer DM, Scuderi MM, Marone C (2016) Laboratory observations of slow earthquakes and the spectrum of tectonic fault slip modes. Nat Commun 7:11104

Li B, Jiang Y, Koyama T, Jing L, Tanabashi Y (2008) Experimental study of the hydro-mechanical behavior of rock joints using a parallel-plate model containing contact areas and artificial fractures. Int J Rock Mech Min Sci 45(3):362–375

Liu J, Polak A, Elsworth D, Grader A (2005) Dissolution-induced preferential flow in a limestone fracture. J Contam Hydrol 78(1–2):53–70

Manga M, Beresnev I, Brodsky EE, Elkhoury JE, Elsworth D, Ingebritsen SE, Mays DC, Wang CY (2012) Changes in permeability caused by transient stresses: field observations, experiments, and mechanisms. Rev Geophys 50(2):RG2004

Marone C (1997) On the rate of frictional healing and the constitutive law for time- and slip-dependent friction. Int J Rock Mech Min Sci 34(3–4):187

Marone C, Cox SJ (1994) Scaling of rock friction constitutive parameters: the effects of surface roughness and cumulative offset on friction of gabbro. Pure Appl Geophys 143(1–3):359–385

Moore DE, Lockner DA (2011) Frictional strengths of talc-serpentine and talc-quartz mixtures. J Geophys Res Solid Earth 116:B01403

Polak A, Elsworth D, Yasuhara H, Grader AS, Halleck PM (2003) Permeability reduction of a natural fracture under net dissolution by hydrothermal fluids. Geophys Res Lett 30(20):SDE1

Polak A, Elsworth D, Liu J, Grader AS (2004) Spontaneous switching of permeability changes in a limestone fracture with net dissolution. Water Resour Res 40:W03052

Ruina A (1983) Slip instability and state variable friction laws. J Geophys Res Solid Earth 88(B12):10359–10370

Samuelson J, Spiers CJ (2012) Fault friction and slip stability not affected by $CO_2$ storage: evidence from short-term laboratory experiments on North Sea reservoir sandstones and caprocks. Int J Greenh Gas Control 11:78–90

Scholz CH (1998) Earthquakes and friction laws. Nature 391(6662):37–42

Taron J, Elsworth D (2010) Coupled mechanical and chemical processes in engineered geothermal reservoirs with dynamic permeability. Int J Rock Mech Min Sci 47(8):1339–1348

Verberne BA, Spiers CJ, Niemeijer AR, De Bresser JHP, De Winter DAM, Plumper O (2014) Frictional properties and microstructure of calcite-rich fault gouges sheared at sub-seismic sliding velocities. Pure Appl Geophys 171:2617–2640

Wang C, Elsworth D, Fang Y (2017) Influence of weakening minerals on ensemble strength and slip stability of faults. J Geophys Res Solid Earth 122(9):7090–7110

Whitney DL, Broz M, Cook RF (2007) Hardness, toughness, and modulus of some common metamorphic minerals. Am Mineral 92:281–288

Witherspoon PA, Wang JS, Iwai K, Gale JE (1980) Validity of cubic law for fluid flow in a deformable rock fracture. Water Resour Res 16(6):1016–1024

Wu W, Reece JS, Gensterblum Y, Zoback MD (2017) Permeability evolution of slowly slipping faults in shale reservoirs. Geophys Res Lett 44(22):11368–11375

Yasuhara H (2004) Evolution of permeability in a natural fracture: significant role of pressure solution. J Geophys Res 109:B03204

Yasuhara H, Polak A, Mitani Y, Grader AS, Halleck PM, Elsworth D (2006) Evolution of fracture permeability through fluid-rock reaction under hydrothermal conditions. Earth Planet Sci Lett 244(1–2):186–200

Zhang F, An M, Zhang L, Fang Y, Elsworth D (2019) The role of mineral composition on the frictional and stability properties of powdered reservoir rocks. J Geophys Res Solid Earth 124(2):1480–1497

Zhong Z, Elsworth D, Hu Y (2016) Evolution of strength and permeability in stressed fractures with fluid-rock interactions. Pure Appl Geophys 173(2):525–536

Zimmerman RW, Yeo IW (2000) Fluid flow in rock fractures: from the Navier-Stokes equations to the cubic law. Geophys Monogr Geophys Union 122:213–224

Zimmerman RW, Chen DW, Cook NG (1992) The effect of contact area on the permeability of fractures. J Hydrol 139(1–4):79–96

Zoback MD, Kohli A, Das I, Mcclure MW (2012) The importance of slow slip on faults during hydraulic fracturing stimulation of shale gas reservoirs. In: SPE 155476 presented at the SPE Americas unconventional resources conference, Pittsburgh